ACS APPLIED MATERIALS & INTERFACES

www.acsami.org Research Article

In Situ Foam 3D Printing of Microcellular Structures Using Material Extrusion Additive Manufacturing

Karun Kalia, Benjamin Francoeur, Alireza Amirkhizi, and Amir Ameli*

Cite This: https://doi.org/10.1021/acsami.2c03014 Read Online

ACCESS | Metrics & More | Article Recommendations | Supporting Information

ABSTRACT: A facile manufacturing method to enable the in situ foam 3D printing of thermoplastic materials is reported. An expandable feedstock filament was first made by incorporation of thermally expandable microspheres (TEMs) in the filament during the extrusion process. The material formulation and extrusion process were designed such that TEM expansion was suppressed during filament fabrication. Polylactic acid (PLA) was used as a model material, and filaments containing 2.0 wt % triethyl citrate and 0.0−5.0 wt % TEM were fabricated. Expandable filaments were then fed into a material extrusion additive manufacturing process to enable the in situ foaming of microcellular structures during layer deposition. The mesostructure, cellular morphology, thermal behavior, and mechanical properties of the printed foams were investigated. Repeatable foam prints with highly uniform cellular structures were successfully achieved. The part density was reduced with an increase in the TEM content, with a maximum reduction of 50% at 5.0 wt % TEM content. It is also remarkable that the interbead gaps of mesostructure vanished due to the local polymer expansion during in situ foaming. The incorporation of TEM and plasticizer only slightly lowered the critical temperatures of PLA, that is, glass-transition, melting, and decomposition temperatures. Moreover, with the introduction of foaming, the specific tensile strength and modulus decreased, whereas the ductility and toughness increased severalfold. The results unveil the feasibility of a novel additive manufacturing technology that offers numerous opportunities toward the manufacturing of specially designed structures including functionally graded foams for a variety of applications.

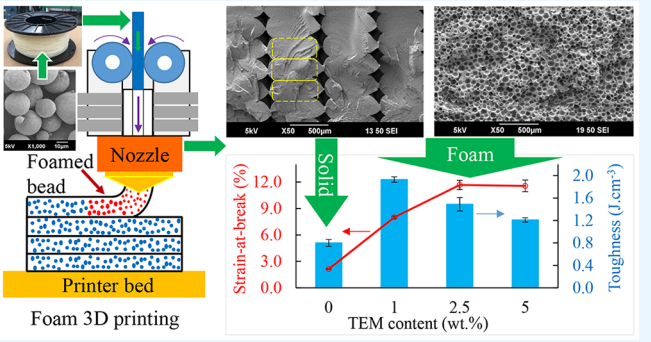

KEYWORDS: *foam, 3D printing, material extrusion additive manufacturing, fused filament fabrication, thermally expandable microsphere, microcellular*

1. INTRODUCTION

Traditional manufacturing methods such as foam injection molding[1−6] and extrusion foaming[7−9] have been extensively studied in regard to material development and novel processing techniques. However, additive manufacturing (AM) of polymeric foams is a recent and emerging field which can integrate the benefits of AM and cellular structures. AM provides great flexibility for designing sustainable, lightweight, and multifunctional parts. Material extrusion AM, *aka* fused filament fabrication or fused deposition modeling, is a highly commercialized manufacturing technology, which provides numerous advantages over traditional manufacturing processes.[10] In the material extrusion AM process, 3D objects are manufactured directly from a computer-aided design model, through layer-by-layer deposition of molten thermoplastic polymers. Compared to traditional manufacturing processes, there are several advantages of the material extrusion AM process such as design freedom, customized products, low-cost manufacturing of complex parts, shorter lead or cycle time, and inexpensive resources.[11−15]

Polymeric foams are some of the most widely used materials, playing an important role in the plastic industry.[7,16−22] Polymeric foams can be manufactured using several methods including physical blowing agents,[7,22] chemical blowing agents,[23−25] and thermally expandable microspheres (TEMs).[26−29] Polymer foams have a very wide range of applications due to their lightweight, flexibility, resistance to impact, high thermal insulation, energy absorption, and damping properties. Foamed materials are thus extensively used in personal protective gear, such as helmets and pads, as well as medical, automotive, aerospace/

Received: February 17, 2022
Accepted: April 26, 2022

defense, construction, and electronic applications. As polymer foams are ubiquitous, the successful integration of AM and polymer foaming provides a unique and creative manufacturing approach with countless applications. Lightweight structural and functional products with complex shapes and graded characteristics[30] (e.g., density and stiffness) can potentially be realized within a printed part. The development of printed cellular structures is, however, in its early stages, and foam 3D printing is emerging.

Overall, three approaches can be used to fabricate foamed parts in the material extrusion AM process: (a) prefoaming, (b) postfoaming,[31−33] and (c) in situ foaming.[34−37] In the prefoaming approach, the feedstock filament is usually foamed during filament fabrication and used as feedstock for 3D printing. The issue with this approach will be the lack of foaming control during the actual printing process, which limits the range of cellular structures that can be obtained. Moreover, it is likely for the premade cells to lose their structure as they pass through the printing process.

In the postfoaming approach, the cellular structure is introduced to the part after the printing is completed. Song et al. reported a method in which gas foaming was applied on 3D-printed parts. Saturation of CO_2 gas in the 3D-printed part was provided using a high-pressure autoclave, followed by depressurization to generate macroporosities.[31] Park et al. also reported the postfoaming of 3D-printed grids made of the copolymer polyethylene terephthalate−polyethylene naphthalate using a similar CO_2 saturation and depressurization approach and studied the compressive and thermal properties of the parts.[32] This approach has several shortcomings: (i) the need for additional expensive and lengthy postprocessing steps of gas impregnation at a relatively high pressure as well as the rapid depressurization device, (ii) difficulty in controlling the part's final shape and dimensions as a fixture may be needed,[31] (iii) limited expansion ranges, and (iv) difficulty of the process scale up.

In situ foam printing is the method that truly integrates the foaming and material extrusion AM processes. In this approach, an unexpanded filament loaded with a blowing agent is first prepared and foam expansion occurs during the printing process, as the filament exits the nozzle. Both physical and chemical blowing agents can be used with this approach. Li et al. reported CO_2 gas-impregnated polyetherimide and polylactic acid (PLA) filaments[34] that were used to print foamed parts. Zhang et al. also demonstrated the preparation of polyurethane foamed scaffolds using a similar approach.[35] The cell nucleation, growth, and stabilization occurred as the CO_2-saturated filament was heated during printing. The challenge with the use of a gas as a blowing agent is the need for an additional gas impregnation step before printing. Moreover, as soon as the gas-saturated filament is removed from the high-pressure chamber, it starts to loose gas quickly.[34] This complicates the storage and handling of gas-impregnated filaments and the widespread application of the process. Damanpack et al. also recently reported 3D-printed PLA foams using filaments loaded with chemical blowing agents[36] and studied the effects of flow rate and print temperature on the part density and mechanical properties. Overall, achieving a uniform polymer/gas solution from a gas or chemical blowing agent during the material extrusion AM process is challenging as it requires longer times and higher pressure levels than what a standard 3D printer can offer. As a result, using a gas or chemical blowing agent usually results in poor cell nucleation, low cell density, and irregular morphology with large cells. In other words, to obtain quality foams with dissolved chemical or physical blowing agents, a specially designed printer system or preprocessing steps are needed.

In contrast, an alternative approach for in situ foam 3D printing could be the use of TEMs,[38−41] which do not require achieving a single-phase polymer/gas solution before cell nucleation and growth. The use of TEM has also proven to provide a more uniform cellular structure in traditional foam processes of extrusion and injection molding, compared to other foaming methods.[26,28,29] This approach does not require any additional preprocess or postprocess steps or a specialized 3D printer machine and can potentially tackle the aforementioned challenges. Andersson et al. recently reported the in situ foam 3D printing of PLA mixed with TEM-ethylene vinyl acetate masterbatch and measured the mechanical strength and morphology of the resultant foams.[37] However, the reported foams exhibited a nonuniform cellular morphology, large variations in densities, brittle behavior, and rough surfaces, which could be attributed to the lack of uniform TEM dispersion as well as material formulation. The morphological nonuniformities could be a consequence of utilizing an extruder incapable of providing sufficient mixing.

Here, we report a new material formulation coupled with a Maddock mixer-equipped pilot-scale single-screw extrusion process that results in printed foams with highly uniform cellular morphologies and repeatable physical and mechanical characteristics. PLA was mixed with 2.0 wt % triethyl citrate (TEC) plasticizer and 0.0−5.0 wt % of acrylonitrile-based TEM with a polyethylene carrier and used as the feedstock material. The unexpanded filaments were fabricated using an optimized extrusion process, followed by in situ foam 3D printing using a commercially available printer machine. The microstructure, cellular morphology, density, thermal behavior, and mechanical properties of the printed foams were thoroughly evaluated and correlated to the level of foam densities and TEM content.

2. EXPERIMENTAL SECTION

Figure 1 shows the overall workflow of the in situ foam printing process, including (a) a scanning electron microscopy (SEM) micrograph of TEM particles used as blowing agents, (b) expandable filament fabricated using a single-screw extrusion, (c) part design and schematic of the in situ foam 3D-printing process, and (d) an example of the printed foam sample.

2.1. Materials. PLA (Ingeo 4043D, NatureWorks), TEM masterbatch (Advancell P501E1, Sekisui with 50 wt % polyethylene carrier), and TEC plasticizer (W308307, MW 276.28 g·mol^{-1}, Sigma-Aldrich), which is miscible in PLA,[42,43] were used in this study. PLA 4043D extrusion grade, provided by NatureWorks, is a relatively high-viscosity resin with a melt flow rate (MFR) of 6 g·10 min^{-1}, a peak melt temperature of 145−160 °C, a glass-transition temperature of 55−60 °C, and a density of 1.24 g·cm^{-3}. TEM P501E1 is a 50% masterbatch with polyethylene carrier with an initial average particle size of 21−31 μm and a bulk density of 1.10 g·cm^{-3}. TEM spherical particles contain low-boiling-point liquid hydrocarbon inside an acrylonitrile copolymer shell. The expansion start temperature (T_{start}) and maximum expansion temperature (T_{max}) of TEM are 160−180 °C and 210−230 °C, respectively. After full expansion, the TEM's density can reach 0.01−0.03 g·cm^{-3}. Isothermal thermogravimetric measurements at 200 °C for 30 min showed that 24 wt% of TEM particles is made of the blowing agent and the rest is shell material. This translates into 0.24, 0.6, and 1.2

https://doi.org/10.1021/acsami.2c03014
ACS Appl. Mater. Interfaces XXXX, XXX, XXX−XXX

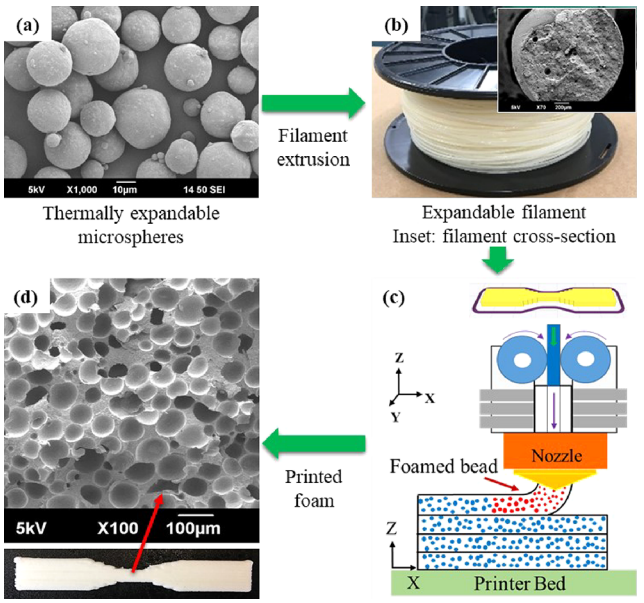

Figure 1. Overview of the in situ foam 3D-printing process: (a) TEM particles as blowing agents, (b) extruded expandable filament with an inset SEM micrograph showing its cross-sectional view, (c) part design and schematic of the in situ foam printing process, and (d) example of the printed tensile sample with a SEM micrograph showing the microcellular morphology in the Y−Z plane.

wt % blowing agents in the examined compositions of PLA/TEC/1.0 wt %TEM, PLA//TEC/2.5 wt % TEM, and PLA/TEC/5.0 wt % TEM, respectively.

2.2. Fabrication of Unexpanded Filaments. Melt blending of PLA/TEC/TEM was conducted to prepare feedstock filaments using a Dr. Collin single-screw extruder (model number: E30P) with a screw diameter of 30 mm and a length to diameter, L/D, ratio of 25. The system is equipped with a Maddock screw profile which is extensively used in the single-screw extrusion process for efficient mixing.[44−46] This mixing capability, together with the use of a masterbatch, promoted the uniform dispersion of the microspheres. The main objective here was to avoid any substantial foaming during filament fabrication. For this purpose, PLA, with an MFR of 6 g·10 min^{-1}, which has a relatively high viscosity and high melt strength was selected. Plasticizer, 2.0 wt % TEC, was dry blended with PLA pellets to tune the PLA's viscosity and melting temperature, such that the extrusion temperatures could be lowered during the filament fabrication process to avoid foaming. With 2.0 wt % TEC, PLA/TEC/TEM compositions were successfully extruded, while the melt temperature (measured right before the die exit) remained below 165 °C. On the one hand, this temperature was high enough to melt PLA and provide a consistent melt flow at pressures below the extruder pressure limit. On the other hand, it was at the low end of TEM's activation temperature range (T_{start}), preventing the TEM expansion and foam occurrence. Also, the rotational screw speed was adjusted so as to yield minimal shear heating but enough to provide good mixing of TEM masterbatch with PLA matrix and stable die pressure. Table 1 lists the processing parameters utilized for the filament fabrication process. The extruded filaments with a diameter of 1.5 ± 0.05 mm were passed through a cold water bath and spooled on Filabot spoolers. It is noted that as there was no upper temperature limitation for PLA and PLA/TEC 2.0 % case, they were extruded at slightly higher temperatures.

2.3. Material Extrusion AM Process. The 3D model for tensile type-V samples was designed according to American Society for Testing and Materials (ASTM) D638 standard.[47] IdeaMaker slicing software was used to convert the model into separate cross-sectional layers that define the printing path (Figure 1c, top). A Raise 3D Pro2 printer, which is capable of providing Z-axis resolution up to 0.01 mm, was used to print foamed and unfoamed samples. Table 2 lists the 3D-printing parameters utilized for printing the samples. The variable parameters were the TEM content as well as the nozzle-exit volumetric flow rate for the case of unfoamed samples. Flow rate adjustment to use partial flow rate is one of the key processing means here to accommodate polymer expansion and density reduction during foaming. For the unfoamed baseline PLA/TEC 2.0% samples, the typical 100% flow rate was employed, while the flow rate for the foams was selected at 85%. The flow rate for all the foamed samples was kept unchanged so that the sole effect of TEM content on the properties of the printed foams could be analyzed. All the samples were printed without an outer shell, and no forced cooling was used during printing.

Table 2. Parameters Utilized in the 3D Printing of Solid and Foam Samples

	variable parameters				
1	TEM content (wt %)	0.0	1.0	2.5	5.0
2	flow rate (%)	100	85	85	85
	fixed parameters				
1	nozzle diameter (mm)	0.8			
2	raster width (mm)	0.8			
3	bed temperature (°C)	55			
4	nozzle temperature (°C)	200			
5	print speed ($mm·s^{-1}$)	25			
6	filling pattern	linear (0°)			
7	layer height (mm)	0.3			
8	infill density (%)	100			

2.4. Characterizations. *2.4.1. Density.* The densities of the filaments and the 3D-printed foam parts were measured using the Mettler Toledo MS303TS/00 density kit as per ASTM D792.[48] The gauge length (narrowed) section of the tensile samples was cut and used for the density measurements. The reported values are the means and standard deviations of three replications in each case. The theoretical densities of the filaments were also calculated using the rule of mixture and the densities of PLA, TEC, PE, and TEM being 1.24, 1.14, 0.97, and 1.10 g·cm^{-3}, respectively.

2.4.2. Microscopy. Optical, scanning electron, and laser confocal microscopy were used for morphological and microstructural investigations. A Dino-Lite AM2111-0.3MP USB digital microscope was used to capture the surface morphology of the printed samples.

Table 1. Single-Screw Extruder Processing Parameters Utilized for Filament Fabrication

	barrel zone temperatures (°C)							
filaments	zone 1	zone 2	zone 3	zone 4	zone 5	screw speed (rpm)	melt temp. before die (°C)	die pressure (bar)
PLA	150	202	199	170	145	8	183 ± 2	117 ± 3
PLA/TEC2.0%	150	202	199	170	145	8	182 ± 2	96 ± 2
PLA/TEC/TEM1.0%	145	155	152	139	127	6	161 ± 2	215 ± 5
PLA/TEC/TEM2.5%	145	155	152	138	127	6	161 ± 2	205 ± 5
PLA/TEC/TEM5.0%	145	155	152	138	126	6	160 ± 2	185 ± 5

https://doi.org/10.1021/acsami.2c03014
ACS Appl. Mater. Interfaces XXXX, XXX, XXX−XXX

Fractured tensile samples, as well as cryo-fractured samples, were used for SEM. The samples were Au sputter-coated (Denton vacuum sputter coater) for 6 min at currents between 3 and 4 mA. The microstructure of coated samples was then observed using SEM (JEOL JSM 6390) under an acceleration voltage of 5 kV. An Olympus LEXT OLS5000 laser confocal microscope was used to reveal foam morphologies on the sample surface.

2.4.3. Cell Size and Cell Density. SEM micrographs taken in Y−Z view (from Figure 1c) of cryo-fractured print samples were used to study the cellular morphologies and measure the cell size and cell density. The image processing was carried out using MIPAR image analysis software. The cell density was measured using the following equation

$$N = \left(\frac{n}{A}\right)^{3/2}$$

where n is the number of cells in the micrograph, A is the area of micrograph in square centimeters, and N is the cell density in number of cells per cubic centimeter (cells·cm^{-3}). The mean and standard deviation of the cell size and the cell density were calculated from at least three SEM images obtained from three sample replicates.

2.4.4. Thermal Properties. Thermogravimetric analysis, TGA, was conducted on the printed samples using a TA Instruments Discovery TGA (S/N 1-0165) system to analyze their thermal stability. Printed samples were heated from 40 to 600 °C with a heating rate of 20 °C·min^{-1}. For TGA testing, platinum pans were used. Each sample had a mass of 7−8 mg. Testing was conducted under a nitrogen atmosphere, and the gas flow rate was kept at 25 mL·min^{-1}.

TA Instruments Discovery differential scanning calorimetry, DSC (S/N 1-0188), was utilized to evaluate the thermal properties of the 3D-printed samples. Samples, weighing 5−6 mg, were hermetically sealed in aluminum pans, and a heating cycle was applied at a rate of 5 °C·min^{-1}. A temperature sweep was done between 0 and 170 °C in a nitrogen atmosphere of 50 mL·min^{-1} flow rate.

TA Instrument's Trios software was used to analyze both DSC and TGA data. The degree of crystallinity (χ_c) was calculated using the following equation

$$\chi_c = \frac{\Delta H_m - \Delta H_{cc}}{\Delta H_m^\circ} \times 100\%$$

where ΔH_m and ΔH_{cc} are the melting enthalpy and the cold crystallization enthalpy, respectively. ΔH_m° is the theoretical melting enthalpy of 100% crystalline PLA, that is, 93 J·g^{-1}.[49] It is noted that only the PLA weight fraction was used in the case of PLA/TEM compositions and the enthalpy values were adjusted in the equation for the true PLA mass.

2.4.5. Tensile Testing. According to the ASTM D638 standard,[47] type-V tensile samples were used for mechanical characterization. An Instron 5966 load frame with a load cell capacity of 10 kN was used with a crosshead displacement speed of 10 mm·min^{-1}. Four samples were tested under each condition, and the average and standard deviation of the mechanical properties are reported. Toughness was calculated as the area under the curve of stress−strain plots until the strain-at-break.

3. RESULTS AND DISCUSSION

3.1. Unexpanded Filaments. Overall, the fabricated filaments showed consistent density (Table 3) and diameter (1.5 ± 0.05 mm) with good cross-sectional circularity. Figure 2a−d shows the SEM micrographs taken from the cross sections of extruded filaments containing 0.0−5.0 wt·% TEM. The very low standard deviation of density measurements (less than 0.6% of the mean) indicates the relatively uniform and consistent dispersion of TEM particles, as it is also evident from Figure 2b−d. No significant difference was observed between the experimentally measured and theoretically calculated density values of the PLA/TEC/TEM filaments; the measured densities were lower than the theoretical values only by 1−4.5%, which could possibly be due to the expansion of some scarce particles or the existence of other types of voids. This range of density drop is however negligible compared to the density ranges of interest in foams, indicating the insignificant expansion of TEM particles. Moreover, as seen in Figure 2b−d, the size of TEM particles is around 20−30 μm, which agrees well with the particle size distribution of as-received TEM particles, provided by the manufacturer. These observations indicate that the majority of the TEM particles remained unexpanded during the filament fabrication.

Table 3. Measured and Theoretical Densities of PLA/TEC/TEM Filaments

TEM (wt %)	measured density (g·cm^{-3})	theoretical density (g·cm^{-3})
0.0	1.232 ± 0.007	1.238
1.0	1.218 ± 0.008	1.234
2.5	1.221 ± 0.003	1.227
5.0	1.167 ± 0.004	1.218

Furthermore, Figure 2 shows that the number of TEM particles increases as the TEM content is increased. It is also seen that the TEM particles were pulled out as intact microspheres and did not fail during the sample cryo-fracture process. The intactness of microspheres is likely due to their relatively thick shells, which constitutes about 75 wt % of the microspheres, according to TGA measurements, and their highly elastic behavior.

3.2. Mesostructure and Microcellular Morphology of 3D-Printed Foams. Figure 3a−d depicts the SEM micrographs of 3D-printed samples with four different compositions: (a) PLA/TEC2.0% (unfoamed), (b) PLA/TEC/TEM1.0%, (c) PLA/TEC/TEM2.5%, and (d) PLA/TEC/TEM5.0%. The view of micrographs in Figure 3 is parallel to the print direction (i.e., X−Z view in Figure 1c) to reveal the rasters in their axial direction. Similarly, Figure 4a−d shows the microstructure of the same material compositions but in a view normal to the print direction (i.e., Y−Z view in Figure 1c), revealing the rasters' cross sections. A remarkable observation from Figures 3 and 4 is the evolution of the print mesostructure, upon the introduction of foaming and increasing the TEM content. As seen in Figures 3a and 4a, large interbead gaps with diamond-shaped cross sections are formed along the print direction during the 3D printing of unfoamed PLA/TEC2.0%. Such gaps were even visible on the part surface (Figures S1a and S2a). This is a characteristic of the material extrusion AM process as repeatedly reported,[15,50−54] which is due to the stacking of extruded cylindrical beads that naturally tend to take a curved cross-sectional form as the material flows out of the nozzle.

The mesostructure was however significantly altered as foaming was introduced to the beads during printing. At PLA/TEC/TEM1.0% foam, the interbead gaps were significantly reduced in cross-sectional size (Figure 4b), but the gap lines were still visible inside the part (Figure 3b) as well as on the surface (Figure S2b). At PLA/TEC/TEM2.5%, the interbead gaps were hardly identifiable (Figures 3c and 4c) and at PLA/TEC/TEM5.0%, they fully vanished (Figures 3d and 4d). With the introduction of in situ foaming, the extruded raster expands as the melt is deposited on top of the

https://doi.org/10.1021/acsami.2c03014
ACS Appl. Mater. Interfaces XXXX, XXX, XXX−XXX

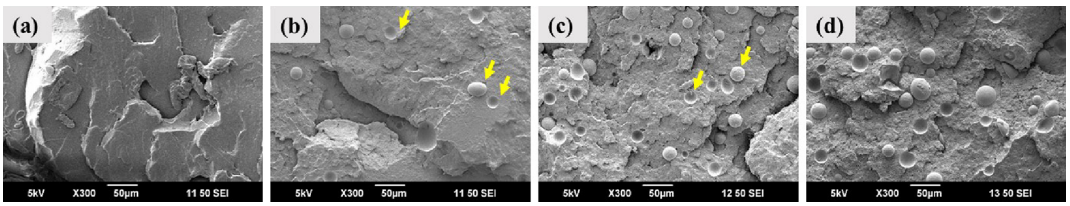

Figure 2. SEM micrographs showing the cross sections of extruded feedstock filaments of PLA/TEC/TEM filaments with (a) 0.0, (b) 1.0, (c) 2.5, and (d) 5.0 wt·% TEM contents.

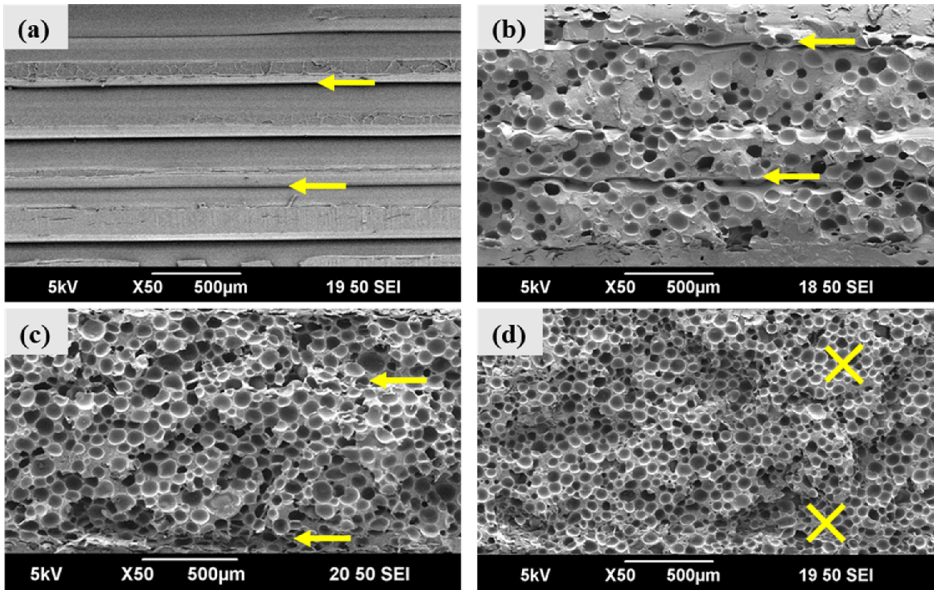

Figure 3. SEM micrographs taken parallel to the print direction ($X-Z$ view in Figure 1c), of (a) PLA/TEC (unfoamed), (b) PLA/TEC/TEM1.0%, (c) PLA/TEC/TEM2.5%, and (d) PLA/TEC/TEM5.0%. Yellow arrows in (a–c) are visual guides to point the layer-to-layer gaps. Yellow crosses in (d) indicate the top and bottom surface of a layer, but they are uniformly bond to the neighboring layers, leaving no gaps.

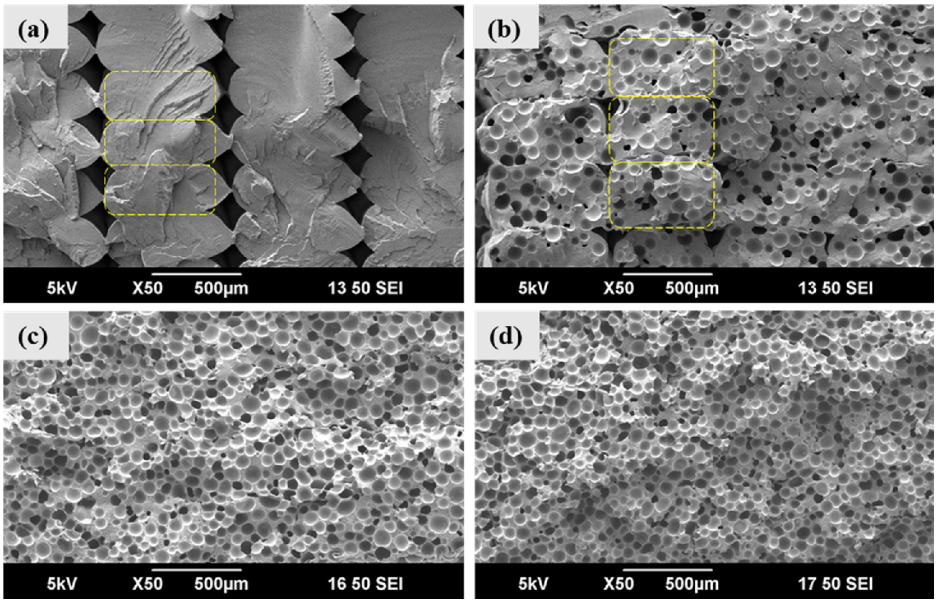

Figure 4. SEM micrographs taken normal to the print direction ($Y-Z$ view in Figure 1c), of (a) PLA/TEC (unfoamed), (b) PLA/TEC/TEM1.0%, (c) PLA/TEC/TEM2.5%, and (d) PLA/TEC/TEM5.0%. Yellow rectangles in (a,b) indicate the cross sections of individual rasters. No such individual raster cross sections were identifiable in (c,d).

underlying raster. This local expansion and resulting pressure upon raster deposition provide an effective mechanism to fill up the free spaces (interbead voids) of the printed structure. Furthermore, with an increase in the TEM content, the cell density and overall foam expansion increase (see Figure 5). This increase in the expansion causes further local pressures

https://doi.org/10.1021/acsami.2c03014
ACS Appl. Mater. Interfaces XXXX, XXX, XXX−XXX

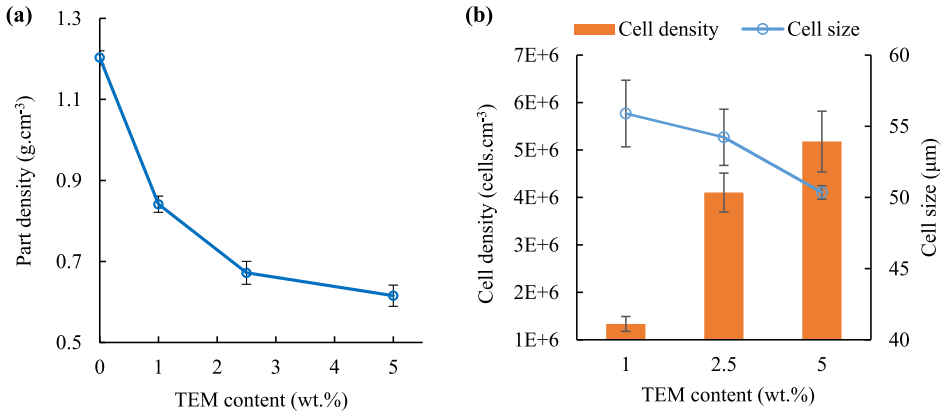

Figure 5. (a) Part density and (b) cell density and cell size of 3D-printed samples as a function of TEM content. Error bars denote ±1 SD (standard deviations).

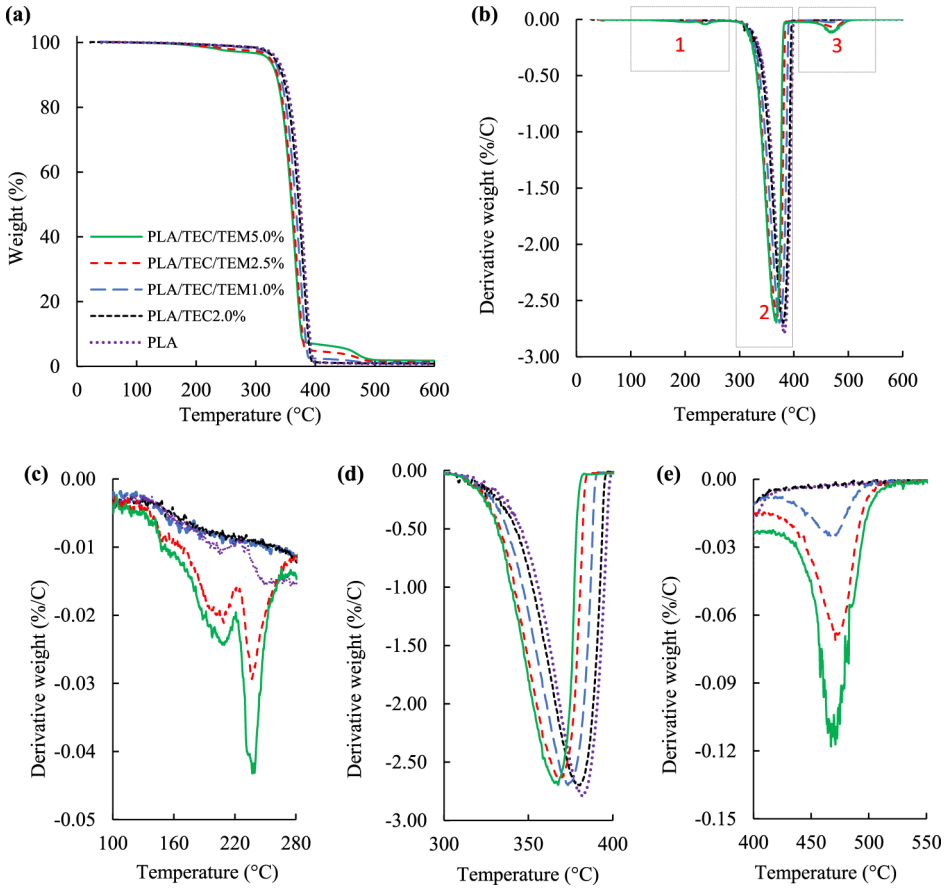

Figure 6. Thermogravimetric data showing the (a) weight loss and (b) derivative weight loss (DTG) at a heating rate of 20 °C·min^{-1} in a nitrogen atmosphere. (c–e) Insets of Figure 6b showing the temperature ranges of 100–280, 300–400, and 400–550 °C, corresponding to Zone 1, Zone 2, and Zone 3, respectively.

and reduction of interbead void size. It can thus be concluded that if a sufficient degree of in situ foam expansion is provided during raster deposition, it can compensate for the free spaces created due to geometrical restrictions of the depositing raster and erase the layering pattern (interbead voids), which can consequently result in a more monolithic and isotropic structure. This could potentially help enhance the transverse properties of parts prepared using the material extrusion AM method.

Another important observation from Figures 3 and 4 is the capability of this method in achieving foam structures with relatively uniform cellular morphologies, especially at high TEM contents. It is interesting to note that relatively circular cross sections of the cells were observed in both views, that is, perpendicular and parallel to the print direction. This indicates that the cells isotropically expanded during the printing process and preserved their spherical shape, with minimal cell elongation. This is usually challenging to achieve in traditional processes such as foam injection molding, especially when using a dissolved physical or chemical blowing agent.[2,5,55]

https://doi.org/10.1021/acsami.2c03014
ACS Appl. Mater. Interfaces XXXX, XXX, XXX–XXX

Table 4. TGA Data for PLA, PLA/TEC, and PLA/TEC/TEM Printed Foams Listing the Decomposition Temperatures and Residue for Zones 1−3 of Figure 6b[a]

	zone 1	zone 2			zone 3	
	T_{max} (°C)	$T_{onset\text{-}5\%}$ (°C)	T_{max} (°C)	$T_{end\text{-}95\%}$ (°C)	T_{max} (°C)	residue (%) at 600 °C
PLA		335.82	382.09	393.24	–	0.76
PLA/TEC2%		331.85	380.69	390.58		0.87
PLA/TEC/TEM1.0%	246.58	330.33	372.44	384.26	473.3	1.04
PLA/TEC/TEM2.5%	243.60	327.85	366.79	381.78	474.8	1.39
PLA/TEC/TEM5.0%	247.15	322.07	360.84	378.30	470.7	1.79

[a] $T_{onset\text{-}5\%}$, T_{max}, and $T_{end\text{-}95\%}$ denote the degradation temperature for 5% weight loss, maximum weight loss rate, and 95% weight loss, respectively.

Figure 5a,b shows the part density, cell density, and cell size as a function of TEM content for PLA/TEC/TEM printed foams. With an increase in the TEM content, the part density and the cell size both decreased, while the cell density increased. The density of the unfoamed PLA/TEC2.0% print was measured to be 1.20 g·cm^{-3} which continuously decreased upon the introduction and increase of TEM content, reaching to 0.61 g·cm^{-3} at 5.0 wt % TEM content, accounting for ∼50% density reduction. Compared to the traditional low-pressure and high-pressure foam injection molding processes which typically provide density reductions in the range of 5−30%, achieving 50% density reduction with such a uniform cellular morphology through in situ foam 3D-printing process is significant.

It is also worth noting that there are several advantages of employing in situ foaming over partial infill to reduce the part density: (a) a wider range of density reduction can be achieved with in situ foaming, while the part is still intact; (b) foaming provides a uniformly distributed microstructure which could be beneficial for mechanical performance; (c) printed foams provide a closed-cell structure that yields essentially air-tight parts and offers advantages for impact and thermal insulation applications; and (d) the scale if microstructural features are different. In the partial infill case, the voids are at the raster-size scale which is in the order of several hundred micrometers. The cells in foamed prints are however around 50 μm, and the two different scales can thus be integrated for hierarchical structures.

As seen in Figure 5b, at TEM 1.0 wt %, the cell density was found to be 1.33 × 10^6 cells·cm^{-3} with an average cell size of 55.9 μm. With an increase in the TEM content to 2.5 wt %, the cell density was increased to 4.1 ×10^6 cells·cm^{-3} and the average cell size was slightly decreased to 54.2 μm. At TEM 5.0 wt %, the cell density was further increased to 5.2 × 10^6 cells·cm^{-3} with an average cell size of 50.3 μm. The increase in the cell density with an increase in the TEM content is expected as each TEM particle potentially acts as a precell that could grow during foaming. Hence, a larger number of TEM particles would translate into a greater cell density. Moreover, higher TEM content and larger cell density would result in a greater degree of volumetric expansion and thus further density reduction.

As seen in Figure 5b, the cell size was slightly reduced with an increase in the TEM content. The degree of overall polymer expansion is not only prescribed by the TEM amount; it will also depend on the print conditions, more specifically transient temperature conditions and the pressure that the exiting melt experiences between the nozzle tip and the underlying raster, that is, geometrical constraints. Under prescribed printing conditions (i.e., nozzle exit volumetric flow rate, print speed, distance between the nozzle and underlying raster, nozzle temperature, and bed temperature), the space ahead of the nozzle tip will have a unique combination of external pressure level and cooling kinetics which will control the competition between melt cooling and foam expansion. This circumstance would allow the melt to expand to a certain degree before the temperature drops to a level wherein no further TEM expansion is possible due to the solidification of the TEM shell. Therefore, it is plausible to assume that each individual microsphere will have less opportunity to grow, under the cooling and geometrical constraints, if the number of microspheres is larger. Future studies will be devised to further understand the interactions between material and process and the resultant structures.

3.3. Thermal Properties of 3D-Printed Foams.

3.3.1. Thermogravimetric Analysis. Figure 6a,b shows the weight loss and the derivative weight loss (rate of weight loss with respect to temperature), respectively, for all the printed samples containing 0.0−5.0 wt % TEM in the temperature range of 0−600 °C, obtained by TGA at a heating rate of 20 °C·min^{-1} in a nitrogen atmosphere. Three important temperature zones were identified based on the TGA data, denoted as Zone 1, Zone 2, and Zone 3 in Figure 6b, corresponding to 100−280, 300−400, and 400−550 °C ranges, respectively. Derivative weight loss (DTG) versus temperature in these zones is given in Figure 6c−e. The values of important temperatures and the residual mass at 600 °C are also summarized in Table 4.

Temperature Zone 1 is associated with the loss of the blowing agent. As the temperature was increased from 100 to 280 °C, the weight loss rate of PLA and PLA/TEC2.0% changed only slightly. However, the weight loss rate was proportionally increased with an increase in the TEM content in the foamed samples. As the TEM content increases, the total mass of gaseous hydrocarbon (as the blowing agent) also increases in the material, which results in more gas loss at this temperature range. Moreover, unlike the PLA and PLA/TEC2.0% samples, a peak and a valley were observed in the DTG curves of PLA/TEC/TEM foam samples (Figure 6c) at ∼221−226 and ∼234−243 °C, respectively. The peak (reduction in DTG, Figure 6c) can be associated with the rapid expansion of the microspheres at this temperature range, which is facilitated by the viscosity reduction in the matrix as well as the increased pressure at the microspheres' core. The rapid volume increase can then lower the TEM internal pressure, resulting in a temporary reduction in the mass loss of gas. With further temperature rise, the TEM shell starts to dissociate and collapse, allowing for the easier escape of the gas out of the melt. Once the temperature exceeds ∼225 °C, the acrylonitrile copolymer shell material starts to lose its melt strength which eventually results in the rupture of the shells by high-pressure gas trapped inside.

https://doi.org/10.1021/acsami.2c03014
ACS Appl. Mater. Interfaces XXXX, XXX, XXX−XXX

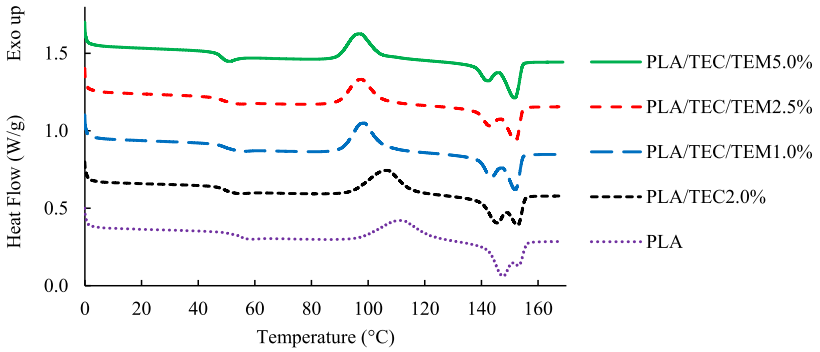

Figure 7. DSC heating thermograms of 3D-printed solid PLA and PLA/TEC2.0% as well as foamed PLA/TEC/TEM samples with varying TEM contents.

Table 5. Thermal Properties and Crystallinity of 3D-Printed Solid PLA and PLA/TEC as Well as Foamed PLA/TEC/TEM Samples with Varying TEM Contents

compositions	T_g (°C)	$T_{c(onset)}$ (°C)	$T_{c(peak)}$ (°C)	ΔH_c (J·g^{-1})	T_{m-1} (°C)	T_{m-2} (°C)	ΔH_m (J·g^{-1})	χ_c (%)
PLA	55.19	97.16	111.51	24.14	147.71	153.41	27.43	3.53
PLA/TEC2.0%	49.65	94.11	106.61	25.59	145.41	152.75	27.70	2.26
PLA/TEC//TEM1.0%	50.24	91.03	98.48	23.37	143.34	151.99	27.82	4.88
PLA/TEC/TEM2.5%	49.24	89.73	97.66	21.43	142.81	152.11	26.34	5.55
PLA/TEC/TEM5.0%	48.17	89.36	97.06	21.74	142.10	151.72	27.55	6.94

Once the shells are ruptured, the gas can escape at a much faster rate and its loss is maximized at the deep valley (~234−243 °C temperature range, Figure 6c).

PLA and TEM shell decomposition occurred in temperature Zone 2 (Figure 6d). The T_{onset} and T_{end} of PLA were found to be 335.82 and 393.24 °C, respectively, similar to the values reported in the literature for a PLA of a similar MFI of 5−7 g·10 min^{-1}.[42] Moreover, the TGA of TEM powder revealed that T_{max} for the decomposition of the TEM shell copolymer is 347.6 °C, which is ~35 °C lower than that of PLA. Overall, the T_{onset}, T_{max}, and T_{end} of PLA were slightly lowered with the incorporation of TEC and TEM, as well as an increase in the TEM content (Table 4). Introducing 2.0 wt % TEC decreased the T_{onset} and T_{end} of PLA by 3~4 °C. With the addition of 1.0 wt % TEM, the T_{onset} and T_{end} decreased to 330.33 and 384.26 °C, respectively, and at TEM 5.0 wt %, the T_{onset} and T_{end} were 322.07 and 378.30 °C, respectively. In other words, the addition of 2.0 wt % TEC and 5.0 wt % TEM masterbatch (5.0 wt % TEM + 5.0 wt % PE) lowered both the T_{onset} and T_{end} of PLA by only ~4%. The decrease in the decomposition temperature of PLA as more TEM was added can be attributed to the slightly lower decomposition temperature of the TEM shell.

Figure 6e shows another weight loss maxima at around 470−473 °C (Zone 3) for PLA/TEC/TEM foam samples, while PLA and PLA/TEC2.0% exhibited a flat DTG in this temperature range. Similar to Figure 6c, the associated valleys were found to be deeper for the higher TEM contents, denoting greater mass loss at higher TEM contents. This mass loss is associated with the decomposition of the PE carrier phase of TEM masterbatch. Moreover, as seen in Table 4, the charred residue at 600 °C increases almost proportionally from 0.87 to 1.79% with an increase in the TEM content from 0.0 to 5.0 wt %. Overall, the mass residue is small and the slight increase in the residue at the presence of TEM could be related to some impurities and inorganic substances present in the TEM masterbatch.

3.3.2. Differential Scanning Calorimetry. Figure 7 shows the DSC first heating thermograms of the printed samples including unfoamed PLA and PLA/TEC2.0% samples as well as foamed PLA/TEC/TEM with varying TEM contents. Table 5 also lists their glass-transition temperature (T_g), the onset and peak temperatures of cold crystallization ($T_{c(onset)}$ and $T_{c(peak)}$), the enthalpies of cold crystallization and melting (ΔH_c and ΔH_m), first and second melting peaks (T_{m1} and T_{m2}), and crystallinity, χ_c. Overall, the critical temperatures were slightly decreased with the introduction of 2.0 wt % TEC plasticizer; the largest drop was observed in T_g which was ~5.5 °C, followed by a decrease in $T_{c(peak)}$ at ~4.9 °C. The drop in T_m values was only ~1−2 °C. TEC plasticizer which is miscible in PLA increases the free volume and results in decreased polymer chain interactions and greater chain mobility at lower temperatures, and consequently, T_g decreases. This increased chain mobility can also result in a better chain packing at lower temperatures and enhance the cold crystallization kinetics which is reflected in the lowered T_c value.

The addition of 1.0−5.0 wt % TEM did not significantly affect the T_g and T_m values; their drop was less than 2 and 3 °C, respectively. T_c was, however, lowered more significantly with the introduction of TEM particles. For instance, $T_{c(peak)}$ was lowered by 8 °C at 1.0 wt % content. Further increase of the TEM content lowered the T_c values only gently. The lower T_c values indicate that the presence of TEM particles enhanced the crystallization kinetics and cold crystallization could take place at lower temperatures. With the introduction of TEM particles, χ_c was consistently increased from 2.26% of the PLA/TEC2.0% sample to 6.94% of the PLA/TEC/TEM5.0% sample. A modest increase in the crystallinity of PLA at the presence of TEM has also been reported in the literature in an extrusion process.[56] Noting that the T_g did not drop significantly with the TEM addition, the increased crystallinity may not be attributed to the increased chain mobility; rather, the TEM particles or polyethylene domains

https://doi.org/10.1021/acsami.2c03014
ACS Appl. Mater. Interfaces XXXX, XXX, XXX−XXX

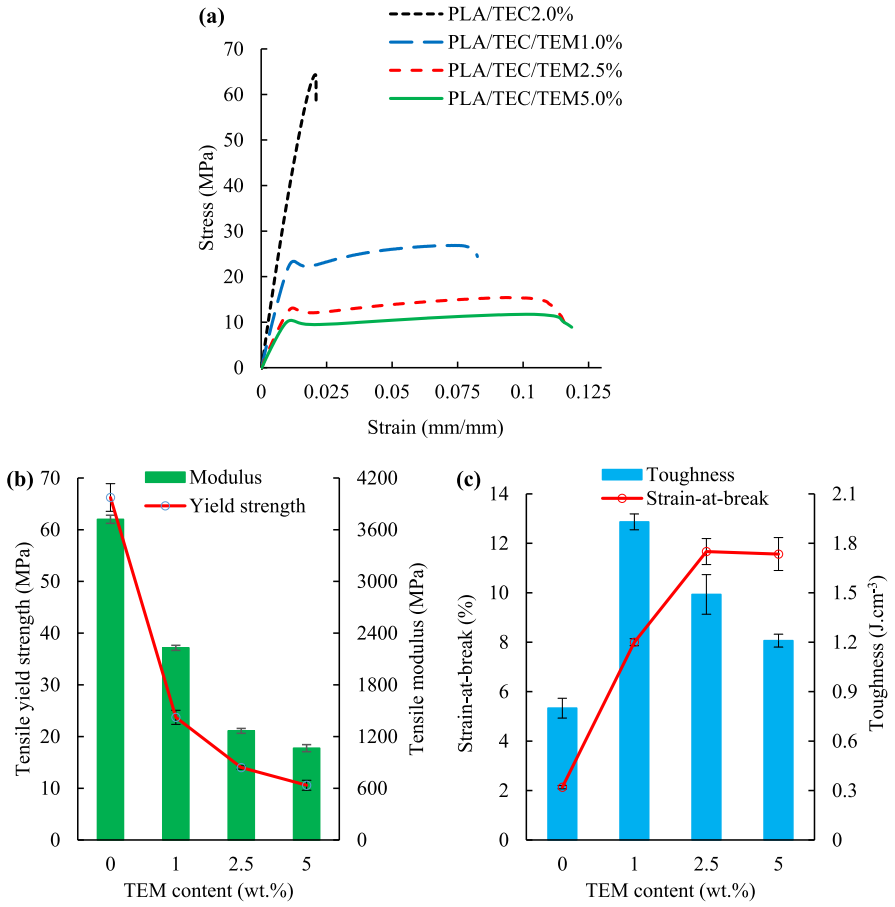

Figure 8. (a) Representative tensile stress−strain graphs of 3D-printed solid and foamed parts. (b) Tensile yield strength and tensile modulus and (c) strain-at-break and toughness, as a function of TEM content. Error bars denote ±1 SD (standard deviations).

might have promoted crystal nucleation.[33,57] This PLA grade can exhibit relatively high degrees of crystallinity under controlled slow cooling conditions. However, overall, the crystallinity of the printed samples was low, indicating that the printing process occurs with a relatively fast cooling. The presence of TEM particles could increase the crystallinity under these fast cooling conditions by about threefold.

3.4. Tensile Properties of 3D-Printed Foams. Figure 8a depicts the representative tensile stress−strain graphs of the printed solid and foam samples. Figure 8b,c also shows the tensile yield strength and tensile modulus as well as strain-at-break and toughness as a function of TEM content. Overall, all the tensile properties were found to be repeatable, evident by small standard deviation values for the replications. This underlines the uniformity and repeatability of the produced expandable filaments and the capability of the material extrusion AM process to provide continuous and uniform in situ foaming. Overall, as the TEM content was increased from 0.0 to 5.0 wt %, which was accompanied with a density reduction of the printed parts (Figure 5a), the strength and modulus values were decreased relatively proportionally, while the strain-at-break and toughness values were increased. Foamed samples exhibited up to 5.5 times increase in the strain-at-break, compared to that of the baseline PLA/TEC2.0% unfoamed sample. This indicates a brittle to ductile transition in the failure mode of the printed PLA once it is foamed, which is generally a desirable mechanical characteristic for applications involving foams.

In order to directly compare the mechanical performance of various samples, their specific mechanical properties, normalized with respect to their density values, were calculated and are summarized in Table 6. With an increase in the TEM content from 0.0 to 5.0 wt %, the specific yield strength and specific modulus values were decreased, accounting for 68 and 44% drop, respectively, at 5.0 wt % TEM. Whereas at 1.0 wt % TEM content, the toughness and the specific toughness values were found to be the largest, that is, 1.93 J·cm^{-3} and 2.29 J·g^{-1}, respectively, which are 141 and 247% higher than those of the baseline PLA/TEC2.0% unfoamed sample. With further increase in the TEM content, the toughness and the specific toughness values dropped slightly due to a reduction in the strength and stiffness. Yet, they were significantly higher than those for unfoamed samples. Overall, the higher toughness values of the foamed

Table 6. Specific Yield Strength, Tensile Modulus, and Toughness of Printed Samples

	specific yield strength (MPa·cm^3·g^{-1})	specific tensile modulus (MPa·cm^3·g^{-1})	specific toughness (J·g^{-1})
PLA/TEC2.0%	55.05	3093.18	0.66
PLA/TEC/TEM1.0%	28.21	2654.76	2.29
PLA/TEC/TEM2.5%	20.90	1889.55	2.09
PLA/TEC/TEM5.0%	17.24	1731.71	1.96

https://doi.org/10.1021/acsami.2c03014
ACS Appl. Mater. Interfaces XXXX, XXX, XXX−XXX

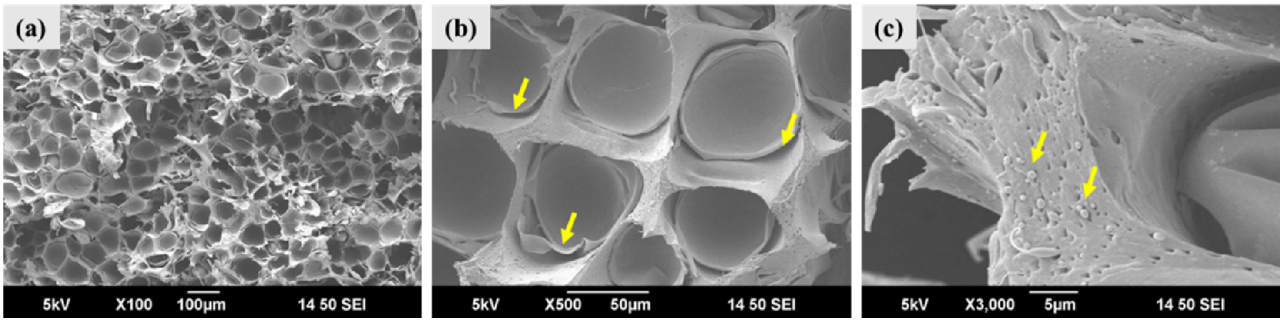

Figure 9. SEM micrographs of the PLA/TEC/TEM5.0% sample that failed under tensile loading at room temperature at magnifications of (a) 100, (b) 500, and (c) 3000.

samples represent their higher energy absorption capacity, which is very appealing for many foam applications.

Figure 9 shows the SEM micrographs of fractured surfaces of a PLA/TEC/TEM 5.0% tensile sample at three different magnifications. The significant plastic deformation beyond elastic yielding is clearly observable in Figure 9a,b, where fibrillar pullouts are seen and the cross-sectional shape of the microspheres is deformed; they are no longer consistently circular, in contrast to what is seen in Figures 3b–d and 4b–d, which was obtained by a brittle failure under liquid nitrogen cryo-fracturing. The evolution of the PLA/TEC/TEM samples' ductility upon the introduction of TEM particles and foaming may be attributed to several factors: (a) the existence of the cellular structure,[58] (b) the stretchable behavior of the acrylonitrile copolymer shell material,[38] and (c) the high ductility of the polyethylene phase from TEM masterbatch carrier.[59,60] Similar behavior, that is, an increase in the strain-at-break with an increase in the TEM content of PLA/TEM, has been reported for injection-molded samples in the literature.[26] Also, Figure 9c shows the dispersed polyethylene phase with a domain size in the range of a few micrometers in the form of deformed and stretched zones, indicating their plastic deformation during tensile testing.

The drop in the specific yield strength and modulus can be attributed to several factors. First, the lack of perfect bonding between the TEM shell surface and PLA phase; as Figure 9b shows, even though the complete delamination between the shell and PLA matrix was not the major failure mechanism (i.e., no TEM particle pull-outs), a separation between the two is frequently observed. A proper choice of compatibilizer can address this issue and enhance the shell/matrix adhesion. Second, the lower modulus and strength of the polyethylene phase, introduced as the TEM carrier, might have contributed to the lowered strength and stiffness of the foams. A proper choice of masterbatch carrier or direct introduction of TEM particles during the filament fabrication process may address this issue.

4. CONCLUSIONS

An economical and scalable manufacturing method that enables the in situ foam 3D printing of thermoplastic materials was reported, revealing the importance of material formulation, filament fabrication process, as well as printing process to achieve repeatable and uniform printed foams. Expandable feedstock filaments were fabricated with the incorporation of TEM-PE in a PLA matrix together with TEC plasticizer during the extrusion process. With the use of a special screw profile and optimized extrusion parameters, unexpanded PLA/TEC/TEM filaments were successfully extruded containing up to 5.0 wt % TEM. Filaments were then fed into a material extrusion AM process to produce foamed parts with uniform microcellular morphologies. With an increase in the TEM content, the cell density and the degree of expansion both increased, whereas the cell size was slightly decreased. At 5.0 wt % TEM content, a 50% density reduction was achieved. Moreover, due to the volumetric expansion during the in situ foaming, the interbead gaps of the mesostructure faded away providing a more homogeneous structure.

Based on the TGA results, compared to the baseline PLA/TEC2.0% samples, the $T_{onset\text{-}5\%}$ and $T_{end\text{-}95\%}$ values were found to decrease by ~3% only upon the addition of 5.0 wt % TEM. From the DSC analysis, T_g and T_{m-2} values only decreased by ~1–2 °C; however, $T_{c(peak)}$ was decreased by 9.5 °C and the crystallinity increased from 2.26 to 6.94%. Overall, the incorporation of TEM did not significantly affect the thermal properties of the printed foams, as compared to the unfoamed parts. TEM particles and PE phase could have acted as crystal nucleating sites thereby enhancing the crystallization kinetics.

Mechanical properties showed very repeatable tensile stress–strain graphs for PLA/TEC/TEM printed foams with varying TEM contents. Compared to the baseline PLA/TEC2.0% samples, the specific tensile yield strength and modulus decreased by 68 and 44%, respectively, at 5.0 wt % TEM content. Whereas the strain-at-break, toughness, and specific toughness all increased. The strain-at-break and specific toughness were enhanced by a maximum of 5.5 and 3.5 times, denoting the high energy absorption capacity of the printed foams. The transition from brittle to ductile failure upon foaming was attributed to the presence of the cellular structure, viscoelastic behavior of the acrylonitrile copolymer TEM shell material, and the ductile behavior of the polyethylene carrier.

This study reports the applicability of a facile AM technology that can offer enormous opportunities toward the manufacturing of customized foams including complex geometrical designs and functionally graded structures for a variety of applications.

■ ASSOCIATED CONTENT

Supporting Information

The Supporting Information is available free of charge at https://pubs.acs.org/doi/10.1021/acsami.2c03014.

https://doi.org/10.1021/acsami.2c03014
ACS Appl. Mater. Interfaces XXXX, XXX, XXX–XXX

Optical and laser confocal microscopy micrographs revealing the surface quality and features of all the printed samples (PDF)

AUTHOR INFORMATION

Corresponding Author

Amir Ameli − *Department of Plastics Engineering, University of Massachusetts Lowell, Lowell, Massachusetts 01854, United States;* orcid.org/0000-0002-1616-1162; Email: Amir_Ameli@uml.edu

Authors

Karun Kalia − *Department of Plastics Engineering, University of Massachusetts Lowell, Lowell, Massachusetts 01854, United States;* orcid.org/0000-0002-3752-9026

Benjamin Francoeur − *Department of Mechanical Engineering, University of Massachusetts Lowell, Lowell, Massachusetts 01854, United States;* orcid.org/0000-0002-8044-7798

Alireza Amirkhizi − *Department of Mechanical Engineering, University of Massachusetts Lowell, Lowell, Massachusetts 01854, United States;* orcid.org/0000-0002-3914-5819

Complete contact information is available at: https://pubs.acs.org/10.1021/acsami.2c03014

Funding

This work was supported by the National Science Foundation under grant number 1822147 [Center for Science of Heterogeneous Additive Printing of 3D Materials (SHAP3D)] and the SHAP3D I/UCRC Members. Any opinions, findings, and conclusions or recommendations expressed in this material are those of the author(s) and do not necessarily reflect the views of the National Science Foundation or SHAP3D members.

Notes

The authors declare no competing financial interest.

ACKNOWLEDGMENTS

The authors thank NatureWorks LLC and Sekisui Chemical Co. Ltd. for providing materials.

REFERENCES

(1) Ameli, A.; Jung, P. U.; Park, C. B. Electrical Properties and Electromagnetic Interference Shielding Effectiveness of Polypropylene/Carbon Fiber Composite Foams. *Carbon* **2013**, *60*, 379−391.

(2) Ameli, A.; Jahani, D.; Nofar, M.; Jung, P. U.; Park, C. B. Development of High Void Fraction Polylactide Composite Foams Using Injection Molding: Mechanical and Thermal Insulation Properties. *Compos. Sci. Technol.* **2014**, *90*, 88−95.

(3) Wu, H.; Zhao, G.; Wang, G.; Zhang, W.; Li, Y. A New Core-Back Foam Injection Molding Method with Chemical Blowing Agents. *Mater. Des.* **2018**, *144*, 331−342.

(4) Wu, H.; Zhao, G.; Wang, J.; Wang, G.; Zhang, W. Effects of Process Parameters on Core-Back Foam Injection Molding Process. *Express Polym. Lett.* **2019**, *13*, 390−405.

(5) Villamil Jiménez, J. A.; Le Moigne, N.; Bénézet, J.-C.; Sauceau, M.; Sescousse, R.; Fages, J. Foaming of PLA Composites by Supercritical Fluid-Assisted Processes: A Review. *Molecules* **2020**, *25*, 3408.

(6) Ameli, A.; Nofar, M.; Jahani, D.; Rizvi, G.; Park, C. B. Development of High Void Fraction Polylactide Composite Foams Using Injection Molding: Crystallization and Foaming Behaviors. *Chem. Eng. J.* **2015**, *262*, 78−87.

(7) Sauceau, M.; Fages, J.; Common, A.; Nikitine, C.; Rodier, E. New Challenges in Polymer Foaming: A Review of Extrusion Processes Assisted by Supercritical Carbon Dioxide. *Prog. Polym. Sci.* **2011**, *36*, 749−766.

(8) Lee, S. T.; Park, C. B. *Foam Extrusion: Principles and Practice*, 2nd ed.; CRC Press, 2014; pp 267−419.

(9) Lee, S. T.; Kareko, L.; Jun, J. Study of Thermoplastic PLA Foam Extrusion. *J. Cell. Plast.* **2008**, *44*, 293−305.

(10) Gao, W.; Zhang, Y.; Ramanujan, D.; Ramani, K.; Chen, Y.; Williams, C. B.; Wang, C. C. L.; Shin, Y. C.; Zhang, S.; Zavattieri, P. D. The Status, Challenges, and Future of Additive Manufacturing in Engineering. *CAD Comput. Aided Des.* **2015**, *69*, 65−89.

(11) Gibson, I.; Rosen, D.; Stucker, B. *Additive Manufacturing Technologies*; Springer, 2019. DOI: 10.1007/978-981-13-8281-9_2.

(12) Attaran, M. The Rise of 3-D Printing: The Advantages of Additive Manufacturing over Traditional Manufacturing. *Bus. Horiz.* **2017**, *60*, 677−688.

(13) Huang, Y.; Leu, M. C.; Mazumder, J.; Donmez, A. Additive Manufacturing: Current State, Future Potential, Gaps and Needs, and Recommendations. *J. Manuf. Sci. Eng. Trans. ASME* **2015**, *137*, 1−10.

(14) Turner, B. N.; Gold, S. A. A Review of Melt Extrusion Additive Manufacturing Processes: II. Materials, Dimensional Accuracy, and Surface Roughness. *Rapid Prototype J.* **2015**, *21*, 250−261.

(15) Penumakala, P. K.; Santo, J.; Thomas, A. A Critical Review on the Fused Deposition Modeling of Thermoplastic Polymer Composites. *Composites, Part B* **2020**, *201*, 108336.

(16) Nofar, M.; Ameli, A.; Park, C. B. Development of Polylactide Bead Foams with Double Crystal Melting Peaks. *Polymer* **2015**, *69*, 83−94.

(17) Afolabi, L. O.; Ariff, Z. M.; Hashim, S. F. S.; Alomayri, T.; Mahzan, S.; Kamarudin, K.-A.; Muhammad, I. D. Syntactic foams formulations, production techniques, and industry applications: a review. *Integr. Med. Res.* **2020**, *9*, 10698−10718.

(18) Li, M.; Qiu, J.; Xing, H.; Fan, D.; Wang, S.; Li, S.; Jiang, Z.; Tang, T. In-Situ Cooling of Adsorbed Water to Control Cellular Structure of Polypropylene Composite Foam during CO_2 Batch Foaming Process. *Polymer* **2018**, *155*, 116−128.

(19) Pinto, J.; Morselli, D.; Bernardo, V.; Notario, B.; Fragouli, D.; Rodriguez-Perez, M. A.; Athanassiou, A. Nanoporous PMMA Foams with Templated Pore Size Obtained by Localized in Situ Synthesis of Nanoparticles and CO_2 Foaming. *Polymer* **2017**, *124*, 176−185.

(20) Jahani, D.; Ameli, A.; Jung, P. U.; Barzegari, M. R.; Park, C. B.; Naguib, H. Open-Cell Cavity-Integrated Injection-Molded Acoustic Polypropylene Foams. *Mater. Des.* **2014**, *53*, 20−28.

(21) Ameli, A.; Nofar, M.; Wang, S.; Park, C. B. Lightweight Polypropylene/Stainless-Steel Fiber Composite Foams with Low Percolation for Efficient Electromagnetic Interference Shielding. *ACS Appl. Mater. Interfaces* **2014**, *6*, 11091−11100.

(22) Zhai, W.; Jiang, J.; Park, C. B. A Review on Physical Foaming of Thermoplastic and Vulcanized Elastomers. *Polym. Rev.* **2021**, *62*, 95−141.

(23) Sadik, T.; Pillon, C.; Carrot, C.; Reglero Ruiz, J.-A. Dsc Studies on the Decomposition of Chemical Blowing Agents Based on Citric Acid and Sodium Bicarbonate. *Thermochim. Acta* **2018**, *659*, 74−81.

(24) Mondy, L. A.; Celina, M.; Kropka, J. M.; Russick, E.; Rao, R. R. Design of Chemically Blown Epoxy Foams. In *27th World Congress of the Polymer Processing Society*, 2011.

(25) Heck, R. L. A Review of Commercially Used Chemical Foaming Agents for Thermoplastic Foams. *J. Vinyl Addit. Technol.* **1998**, *4*, 113−116.

(26) Peng, J.; Srithep, Y.; Wang, J.; Yu, E.; Turng, L.-S.; Peng, X.-F. Comparisons of microcellular polylactic acid parts injection molded with supercritical nitrogen and expandable thermoplastic microspheres: Surface roughness, tensile properties, and morphology. *J. Cell. Plast.* **2012**, *49*, 33−45.

(27) Zhang, R.-Z.; Chen, J.; Huang, M.-W.; Zhang, J.; Luo, G.-Q.; Wang, B.-Z.; Li, M.-J.; Shen, Q.; Zhang, L.-M. Synthesis and Compressive Response of Microcellular Foams Fabricated from Thermally Expandable Microspheres. *Chin. J. Polym. Sci., Engl. Ed.* **2019**, *37*, 279−288.
(28) Kmetty, Á.; Litauszki, K. Development of Poly (Lactide Acid) Foams with Thermally Expandable Microspheres. *Polymers* **2020**, *12*, 463.
(29) Contreras, V.; Maturana, F. J.; Poveda, J.; Núñez, K. C.; Merino, J. C.; Pastor, J. M. Optimization of Injection Parameters to Obtain Selected Properties on Foamed PP with Hollow Glass Microspheres and Thermally Expandable Microspheres Using Taguchi Method. *J. Cell. Plast.* **2020**, *57*, 313−327.
(30) Li, Y.; Feng, Z.; Hao, L.; Huang, L.; Xin, C.; Wang, Y.; Bilotti, E.; Essa, K.; Zhang, H.; Li, Z.; Yan, F.; Peijs, T. A Review on Functionally Graded Materials and Structures via Additive Manufacturing: From Multi-Scale Design to Versatile Functional Properties. *Adv. Mater. Technol.* **2020**, *5*, 1900981.
(31) Song, P.; Zhou, C.; Fan, H.; Zhang, B.; Pei, X.; Fan, Y.; Jiang, Q.; Bao, R.; Yang, Q.; Dong, Z.; Zhang, X. Novel 3D Porous Biocomposite Scaffolds Fabricated by Fused Deposition Modeling and Gas Foaming Combined Technology. *Composites, Part B* **2018**, *152*, 151−159.
(32) Park, B. K.; Kim, C.-J.; Kwon, D. E.; Lee, Y.-W. Design and Fabrication of Partially Foamed Grid Structure Using Additive Manufacturing and Solid State Foaming. *Processes* **2020**, *8*, 1594.
(33) Wang, J.; Xie, H.; Weng, Z.; Senthil, T.; Wu, L. A Novel Approach to Improve Mechanical Properties of Parts Fabricated by Fused Deposition Modeling. *Mater. Des.* **2016**, *105*, 152−159.
(34) Li, M.; Jiang, J.; Hu, B.; Zhai, W. Fused deposition modeling of hierarchical porous polyetherimide assisted by an in-situ CO_2 foaming technology. *Compos. Sci. Technol.* **2020**, *200*, 108454.
(35) Zhang, S.; Shi, X.; Miao, Z.; Zhang, H.; Zhao, X.; Wang, K.; Qin, J.; Zhang, G. 3D-Printed Polyurethane Tissue-Engineering Scaffold with Hierarchical Microcellular Foam Structure and Antibacterial Properties. *Adv. Eng. Mater.* **2022**, *24*, 2101134.
(36) Damanpack, A. R.; Sousa, A.; Bodaghi, M. Porous PLAs with Controllable Density by FDM 3D Printing and Chemical Foaming Agent. *Micromachines* **2021**, *12*, 866.
(37) Andersson, H.; Örtegren, J.; Zhang, R.; Grauers, M.; Olin, H. Variable Low-Density Polylactic Acid and Microsphere Composite Material for Additive Manufacturing. *Addit. Manuf.* **2021**, *40*, 101925.
(38) Jonsson, M.; Nordin, O.; Kron, A. L.; Malmström, E. Thermally Expandable Microspheres with Excellent Expansion Characteristics at High Temperature. *J. Appl. Polym. Sci.* **2010**, *117*, 384−392.
(39) Cai, J.-H.; Huang, M.-L.; Chen, X.-D.; Wang, M. Thermo-Expandable Microspheres Strengthened Polydimethylsiloxane Foam with Unique Softening Behavior and High-Efficient Energy Absorption. *Appl. Surf. Sci.* **2021**, *540*, 148364.
(40) Gong, W.; Pei, X.; Yin, X.; Ban, D.; Fu, H.; He, L. Synthesis of high-temperature thermally expandable microcapsules and their effects on foaming quality and surface quality of foamed ABS materials. *e-Polymers* **2020**, *20*, 519−527.
(41) Fujino, M.; Taniguchi, T.; Kawaguchi, Y.; Ohshima, M. Mathematical Models and Numerical Simulations of a Thermally Expandable Microballoon for Plastic Foaming. *Chem. Eng. Sci.* **2013**, *104*, 220−227.
(42) Maiza, M.; Benaniba, M. T.; Quintard, G.; Massardier-Nageotte, V. Biobased Additive Plasticizing Polylactic Acid (PLA). *Polimeros* **2015**, *25*, 581−590.
(43) Herrera, N.; Singh, A.; Salaberria, A.; Labidi, J.; Mathew, A.; Oksman, K. Triethyl Citrate (TEC) as a Dispersing Aid in Polylactic Acid/Chitin Nanocomposites Prepared via Liquid-Assisted Extrusion. *Polymers* **2017**, *9*, 406.
(44) Sun, X.; Spalding, M. A.; Womer, T. W.; Uzelac, N. Design Optimization of Maddock Mixers for Single-Screw Extrusion Using Numerical Simulation. In *ANTEC 2017, Conference Proceedings*; Society of Plastics Engineers, 2017; pp 1017−1023.
(45) Podyman, H. S.; Dvoinos, Y. H.; Novik, V. A. Modeling the Homogenization Process of Polyethylene Compositions in a Single-Screw Extruder with a Maddock Mixing Element. *Mech. Compos. Mater.* **2021**, *57*, 517−526.
(46) Hopmann, C.; Schön, M.; Reul, M. M.; Facklam, M. A Method for the Validation of Simulated Mixing Characteristics of Two Dynamic Mixers in Single-Screw Extrusion. *Polymers* **2020**, *12*, 2234.
(47) *ASTM D638-14: Standard Test Method for Tensile Properties of Plastics*; ASTM, 2014.
(48) *ASTM D792-13: Standard Test Methods for Density and Specific Gravity (Relative Density) of Plastics by Displacement*; ASTM, 2008.
(49) Saha, D.; Samal, S. K.; Biswal, M.; Mohanty, S.; Nayak, S. K. Preparation and Characterization of Poly(Lactic Acid)/Poly-(Ethylene Oxide) Blend Film: Effects of Poly(Ethylene Oxide) and Poly(Ethylene Glycol) on the Properties. *Polym. Int.* **2019**, *68*, 164−172.
(50) Sood, A. K.; Ohdar, R. K.; Mahapatra, S. S. Parametric Appraisal of Mechanical Property of Fused Deposition Modelling Processed Parts. *Mater. Des.* **2010**, *31*, 287−295.
(51) Blok, L. G.; Longana, M. L.; Yu, H.; Woods, B. K. S. An Investigation into 3D Printing of Fibre Reinforced Thermoplastic Composites. *Addit. Manuf.* **2018**, *22*, 176−186.
(52) Kalia, K.; Ameli, A. Effect of Carbon Fiber on the Fracture Toughness of Fused Filament Fabricated CF/ABS Composites. In *ANTEC 2021, Conference Proceedings*; Society of Plastics Engineers, 2021.
(53) Arif, M. F.; Kumar, S.; Varadarajan, K. M.; Cantwell, W. J. Performance of Biocompatible PEEK Processed by Fused Deposition Additive Manufacturing. *Mater. Des.* **2018**, *146*, 249−259.
(54) Spoerk, M.; Arbeiter, F.; Cajner, H.; Sapkota, J.; Holzer, C. Parametric Optimization of Intra- and Inter-Layer Strengths in Parts Produced by Extrusion-Based Additive Manufacturing of Poly(Lactic Acid). *J. Appl. Polym. Sci.* **2017**, *134*, 45401.
(55) Kuang, T.-R.; Mi, H.-Y.; Fu, D.-J.; Jing, X.; Chen, B.-y.; Mou, W.-J.; Peng, X.-F. Fabrication of Poly(Lactic Acid)/Graphene Oxide Foams with Highly Oriented and Elongated Cell Structure via Unidirectional Foaming Using Supercritical Carbon Dioxide. *Ind. Eng. Chem. Res.* **2015**, *54*, 758−768.
(56) Litauszki, K.; Kmetty, Á. Investigation of the Damping Properties of Polylactic Acid-Based Syntactic Foam Structures. *Polym. Test.* **2021**, *103*, 107347.
(57) Khonakdar, H. A. Dynamic Mechanical Analysis and Thermal Properties of LLDPE/EVA/Modified Silica Nanocomposites. *Composites, Part B* **2015**, *76*, 343−353.
(58) Sun, X.; Kharbas, H.; Peng, J.; Turng, L.-S. A Novel Method of Producing Lightweight Microcellular Injection Molded Parts with Improved Ductility and Toughness. *Polymer* **2015**, *56*, 102−110.
(59) Quitadamo, A.; Massardier, V.; Santulli, C.; Valente, M. Optimization of Thermoplastic Blend Matrix HDPE/PLA with Different Types and Levels of Coupling Agents. *Materials* **2018**, *11*, 2527.
(60) Madhu, G.; Bhunia, H.; Bajpai, P. K. Blends of High Density Polyethylene and Poly(L-Lactic Acid): Mechanical and Thermal Properties. *Polym. Eng. Sci.* **2014**, *54*, 2155−2160.

https://doi.org/10.1021/acsami.2c03014
ACS Appl. Mater. Interfaces XXXX, XXX, XXX−XXX